



Commissioning of the LaBr₃(Ce) detector array at the National Superconducting Cyclotron Laboratory

B. Longfellow^{a,b,*}, P.C. Bender^{a,1}, J. Belarge^{a,2}, A. Gade^{a,b}, D. Weisshaar^a

^a National Superconducting Cyclotron Laboratory, Michigan State University, East Lansing, MI 48824, USA

^b Department of Physics and Astronomy, Michigan State University, East Lansing, MI 48824, USA

ARTICLE INFO

Keywords:

LaBr₃(Ce) scintillators
Fast-timing arrays
Lifetime measurements
Angular correlation measurements

ABSTRACT

The timing and energy resolution properties of LaBr₃(Ce) scintillators are well suited for use in $\gamma\gamma$ fast-timing experiments. Using standard ⁶⁰Co, ⁸⁸Y, and ¹⁵²Eu sources, the 16-element array of 1.5 inch \times 1.5 inch right-cylindrical LaBr₃(Ce) detectors and the associated readout electronics at the National Superconducting Cyclotron Laboratory were commissioned by measuring the lifetimes of excited states and the angular correlations of γ rays emitted in cascade. Excited-state lifetimes in ¹⁵²Sm and ¹⁵²Gd were measured using the exponential slope of the decay and a method based on the centroids of time-difference spectra. Results for the lifetimes are consistent with the well-known literature values which cover a range from a few picoseconds to several nanoseconds. Furthermore, the $\gamma\gamma$ angular correlations for the $4^+ \rightarrow 2^+ \rightarrow 0^+$ cascade in ⁶⁰Ni and the $3^- \rightarrow 2^+ \rightarrow 0^+$ cascade in ⁸⁸Sr were measured and shown to agree with GEANT4 simulations that take into account the expected angular correlations within the cascades as well as the geometry of the array.

1. Introduction

The lifetime (τ) and the spin-parity (J^π) of a nuclear excited state are important properties in nuclear structure physics. The reduced electromagnetic transition probability between two bound nuclear states — $B(\sigma\lambda; J_i^\pi \rightarrow J_f^\pi)$, which depends on the multipolarity $\sigma\lambda$, e.g. $E1$, $E2$, or $M1$, of the corresponding γ -ray transition, is determined by the partial lifetime of the initial state. This quantity is a sensitive probe of the wave functions of the states involved and characterizes collective phenomena such as rotations and vibrations. Consequently, measurements of excited-state lifetimes and multiplicities provide useful benchmarks for theoretical nuclear structure models.

Recently, the use of the scintillator material LaBr₃(Ce) has become popular for direct lifetime measurements via γ -ray spectroscopy at facilities worldwide [1]. The high light output and fast decay-time properties of LaBr₃(Ce) give rise to good energy resolution and excellent timing resolution, allowing precise measurements on the sub-nanosecond scale [2–4]. For example, at IFIN-HH Bucharest, LaBr₃(Ce) detectors have been used as part of the LaBr₃(Ce)-HPGe hybrid array ROSPHERE [5,6] and the FAsT-TIMing Array (FATIMA) [7] of LaBr₃(Ce) detectors has

been combined with EXILL at ILL Grenoble [8], with EURICA at RIBF-RIKEN [9,10], and with a silicon detector array to form the STELLA apparatus for nuclear astrophysics measurements at IPN Orsay [11]. The performance of two LaBr₃(Ce) detectors in conjunction with GAMMASPHERE at Argonne National Laboratory was evaluated [12] and FATIMA was used with GAMMASPHERE for fast-timing measurements in ²⁵²Cf fission source data [13,14]. Furthermore, the National Nuclear Array (NANA) of LaBr₃(Ce) detectors at the National Physical Laboratory has been commissioned [15] and used for angular correlation measurements and the absolute activity standardization of a ⁶⁰Co source [16].

At the National Superconducting Cyclotron Laboratory (NSCL) [17], the applicability of LaBr₃(Ce) scintillators to both in-flight and stopped-beam measurements has been demonstrated. Two LaBr₃(Ce) detectors were tested for use in in-beam γ -ray spectroscopy experiments [18], two LaBr₃(Ce) detectors were used in the optimization of the NSCL digital data acquisition system for fast timing [19], and ten LaBr₃(Ce) detectors were used to measure β -delayed γ rays from ions implanted in a plastic scintillator to determine lifetimes in ^{68,70}Ni [20]. Here, we present results from the commissioning of the NSCL's full array of 16 LaBr₃(Ce)

* Corresponding author at: National Superconducting Cyclotron Laboratory, Michigan State University, East Lansing, MI 48824, USA.
E-mail address: longfell@nscl.msu.edu (B. Longfellow).

¹ Present address: Department of Physics and Applied Physics, University of Massachusetts Lowell, Lowell, MA 01854, USA.

² Present address: MIT Lincoln Laboratory, Lexington, MA 02421, USA. No Laboratory funding or resources were used to produce the result/findings reported in this publication.

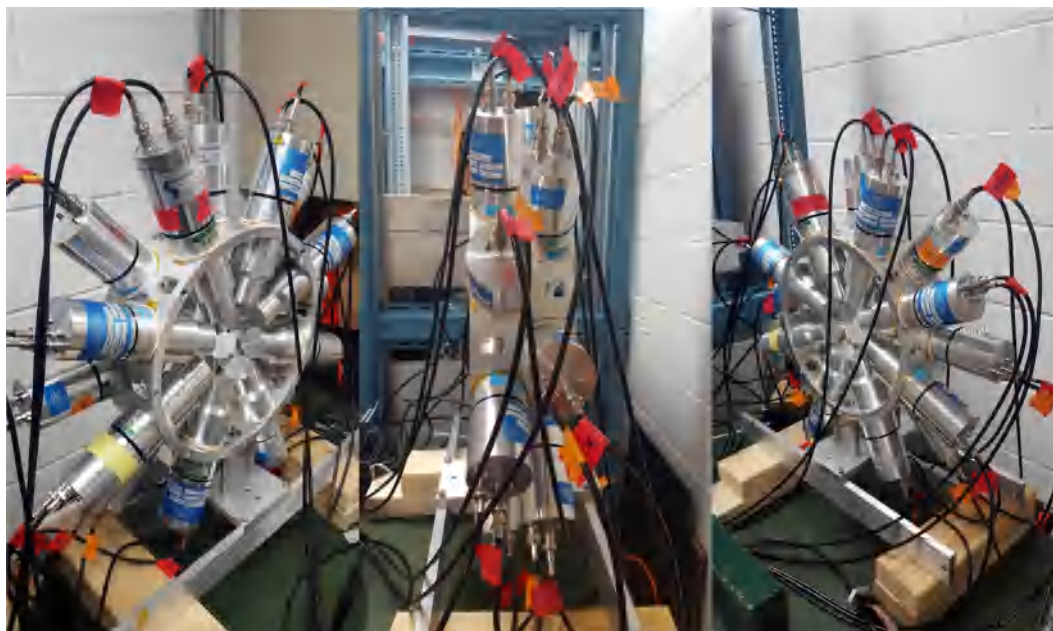


Fig. 1. Pictures of the $\text{LaBr}_3(\text{Ce})$ scintillators arranged in two rings of eight detectors each from different perspectives. The sources used in measurements were placed at the center of the array, equidistant from both rings.

detectors and its dedicated readout electronics through lifetime and angular correlation measurements with ^{60}Co , ^{88}Y , and ^{152}Eu sources.

2. Experimental setup

For the offline commissioning measurements, all 16 Saint-Gobain BrillLanCe 380 $\text{LaBr}_3(\text{Ce})$ scintillators [21] available at the NSCL were utilized. The 1.5 inch \times 1.5 inch right-cylindrical $\text{LaBr}_3(\text{Ce})$ crystals were coupled to Hamamatsu R6231 photomultiplier tubes (PMTs). The PMTs were powered by a WIENER MPOD EHS F020P HV module and operated at positive bias voltages ranging from 600 to 800 V. Voltages were chosen to align the pulse heights for all detectors to the same amplitude. As shown in Fig. 1, the 16 scintillators were placed in an array consisting of two rings of eight detectors each with the rings offset by 1.9 inches center-to-center. The front faces of the detectors were positioned 2.125 inches from the symmetry axis of the rings. For all measurements, the γ -ray sources were located in the center of the array, equidistant from the two rings. For experiments at the NSCL, the depth of the $\text{LaBr}_3(\text{Ce})$ detectors can be adjusted to accommodate the diameter of the cylindrical beam pipe housing the target or implantation detector, depending on the experimental scheme. The small width of the array's frame allows the $\text{LaBr}_3(\text{Ce})$ scintillators to be used in concurrence with other detector arrays while minimizing losses in geometric efficiency. For example, in Ref. [20], the $\text{LaBr}_3(\text{Ce})$ array was placed in between the two rings of the Segmented Germanium Array (SeGA) [22].

The data acquisition system for the array employed the Mesytec MCFD-16, MTDC-32, and MQDC-32 modules [23]. The 16 $\text{LaBr}_3(\text{Ce})$ PMT output signals were connected to the inputs of the MCFD-16, a constant fraction discriminator with a built-in preamplifier and gate generator, via LEMO cables. The delay and fraction for the constant fraction discriminator yielding optimal time resolution were 12 ns and 40%. The same delay and fraction were used for all channels. The 16 ECL timing-gate outputs and 16 amplitude outputs of the MCFD-16 were provided to the MTDC-32 and MQDC-32, respectively, using 34-pin twisted ribbon cables. The OR output (NIM logic signal) of the MCFD-16 was plugged into the gate input of the MQDC-32, a charge-integrating analog-to-digital converter, by LEMO cable to supply the integration gate for the amplitude signals. The Trig output (NIM logic signal) of the MCFD-16 was sent to a gate and delay generator, converted to an ECL signal, and then connected to both the MTDC-32

and MQDC-32 on a shared ribbon cable to provide the “experiment trigger”, which ensures the synchronization of the timing and energy modules and gives the common start for the MTDC-32's time-to-digital conversion. When the $\text{LaBr}_3(\text{Ce})$ array is used in conjunction with other detector systems, the gate and delay generator can be replaced with complex trigger logic to provide an “experiment trigger” derived from all systems of the setup. The delay for the “experiment trigger” gate relative to the prompt $\text{LaBr}_3(\text{Ce})$ signal can be up to 16 μs . The modules were operated in multi-hit mode with the event window for coincidences set to 256 ns and divided into 2^{16} channels, giving a timing dispersion of 1/256 ns (3.90625 ps). See Fig. 2 for a diagram of the electronics setup for the array. The MTDC-32 and MQDC-32 were read out through a VME interface and the data were sorted and analyzed using the GRUTinizer [24] software package, which is built on the ROOT framework. Using the VME busy signal, the livetime of the setup was determined to be greater than 99% for all measurements presented in this work.

3. Excited-state lifetime measurements

To begin, a ^{60}Co standard calibration source was used to investigate the timing performance of the $\text{LaBr}_3(\text{Ce})$ array and electronics setup. ^{60}Co β^- decays with a 99.9% branching ratio to the 2505.7-keV level in ^{60}Ni , which then decays via a cascade of 1173.2 and 1332.5-keV γ rays to the ground state [25]. Since the lifetime of the 1332.5-keV intermediate state is 1.06(3) ps [25], the 310 ps FWHM of the time difference spectrum between coincident 1173.2 and 1332.5-keV γ rays measured with the $\text{LaBr}_3(\text{Ce})$ detectors seen in Fig. 3 provides a characterization of the setup's prompt-timing properties at these energies. The individual time difference spectra for all detector pairs in the array were aligned and then summed to produce Fig. 3. The timing resolution for each detector pair was similar to the 310-ps FWHM of the entire array. As shown in Fig. 14 of Ref. [19], the timing resolution between two of the $\text{LaBr}_3(\text{Ce})$ detectors for 1173.2–1332.5 keV coincidences as measured with the NSCL digital data acquisition system was about 330 ps using detector signals amplified to a large fraction of the input range of the 250 megasamples per second digitizers to optimize performance.

For states with lifetimes much larger than the prompt-timing response of the array, the lifetime can be measured from the slope of the

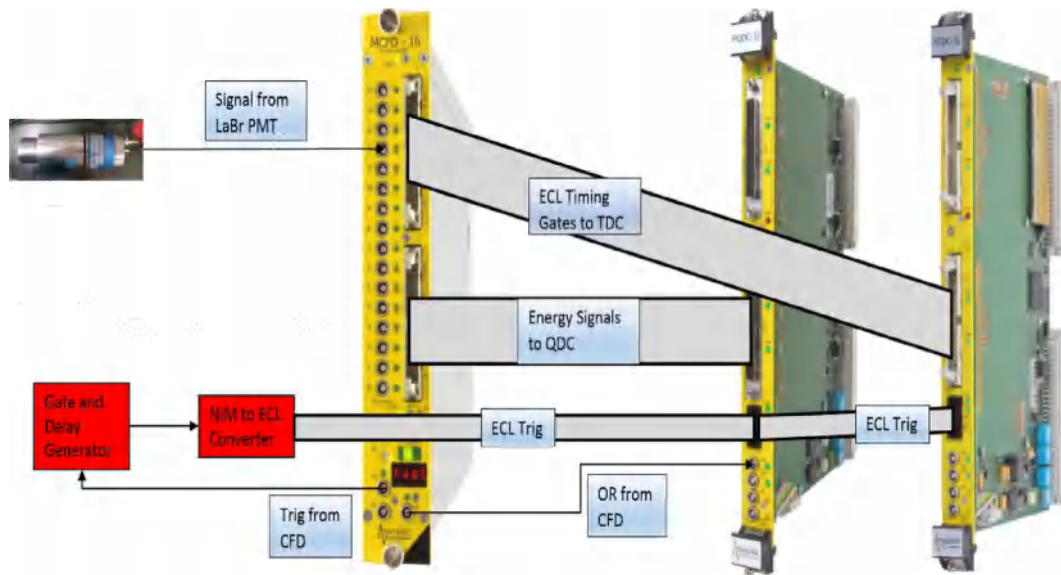


Fig. 2. Diagram of the LaBr₃(Ce) array electronics setup. Times and energies were extracted from LaBr₃(Ce) PMT signals using the Mesytec MCFD-16, MTDC-32, and MQDC-32 modules [23]. When used in conjunction with other detector systems, the gate and delay generator can be replaced with complex trigger electronics to provide the “experiment trigger”, which must be provided to the MTDC-32 and MQDC-32 within about 16 μ s.

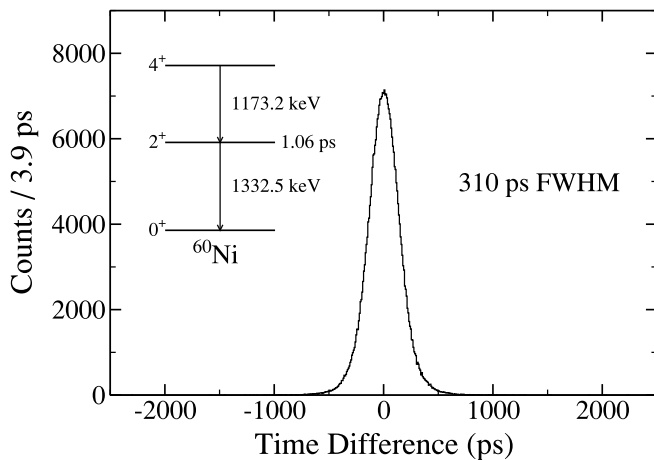


Fig. 3. Time difference spectrum for 1173.2 and 1332.5 keV coincidences following the β^- decay of a standard ^{60}Co source at the center of the array of 16 LaBr₃(Ce) detectors. The stop–start time difference is taken with the 1173.2 keV detection time as the start and the 1332.5 keV detection as the stop. Since the lifetime of the 1332.5-keV state is 1.06 ps, the FWHM of 310 ps is indicative of the array’s prompt-timing response to γ rays of these energies.

exponential decay seen in the time-difference spectrum for $\gamma\gamma$ coincidences. As seen in Fig. 4, several states feeding the 121.8-keV level in ^{152}Sm are populated from decay of a standard ^{152}Eu calibration source through electron capture. The time difference between the detection of a 121.8-keV γ ray in one LaBr₃(Ce) scintillator and the detection of the energy of a feeder γ ray in another LaBr₃(Ce) was plotted and fit with an exponential decay curve to extract the lifetime of the 121.8-keV state for several feeders, as demonstrated in Fig. 5 with 244.7–121.8 keV coincidences. As seen in Table 1, the average result found from all feeders of 2030(20) ps is in good agreement with the known lifetime of 2024(16) ps [26].

If the lifetime of the level of interest is shorter than the energy-dependent timing resolution of the array, it becomes impractical to fit the decay curve with an exponential or a convolution of the prompt-timing response and an exponential. In this case, methods for fast-timing arrays using the centroids of time-difference spectra can be

employed [27,28]. As a test of the array of LaBr₃(Ce) detectors, the lifetimes of several states in ^{152}Sm and ^{152}Gd populated from the electron-capture and β^- decays, respectively, of ^{152}Eu were measured using $\gamma\gamma$ coincidences (see level schemes in Fig. 4). First, the coincidence timing spectra for all detector pairs were aligned by applying constant shifts to each pair of time differences using the 778.9–344.3 keV coincidences in ^{152}Gd as described in Ref. [28]. That is, for each detector pair ij , the time-difference spectra $dt_{ij} = t_i(E_2) - t_j(E_1)$ and $dt_{ji} = t_j(E_2) - t_i(E_1)$ were aligned using $E_2 = 344.3$ keV and $E_1 = 778.9$ keV, within energy tolerances. Using this alignment procedure, an energy–energy–time difference cube for coincident hits for the entire array was constructed by filling the points $(E_x, E_y, dt) = (E_a, E_b, t_b - t_a)$ and $(E_b, E_a, t_a - t_b)$ for each coincidence. As a result, gating on $E_x = 300$ keV and $E_y = 400$ keV, for example, gives the $t_{400} - t_{300}$ time-difference spectrum and gating on $E_x = 400$ keV and $E_y = 300$ keV gives the mirror-symmetric $t_{300} - t_{400}$ time-difference spectrum. An additional global shift was applied so that the time-difference spectra were symmetric about zero. As shown in Ref. [28], the value of the reference time, the point about which the time-difference spectra are symmetric, is energy independent.

We consider a state with lifetime τ that is fed with a γ ray of energy E_f and decays via a γ ray of energy E_d . Choosing E_f, E_d coincidences by gating on $E_x = E_f$ and $E_y = E_d$ in the energy–energy–time difference cube yields the $t_d - t_f$ time-difference spectrum. With the reference time at zero, the centroid of this spectrum $C(t_d - t_f)$ gives the lifetime of the state when corrected by the average, energy-dependent time walk of the setup $TW(E)$ [28]

$$\tau = C(t_d - t_f) - TW(E_d) + TW(E_f). \quad (1)$$

The time-walk curve for the array was calibrated using the well-known lifetimes of states in ^{152}Sm and ^{152}Gd . First, the 411.1–344.3 keV, 778.9–344.3 keV, 1089.7–344.3 keV, and 1299.1–344.3 keV $\gamma\gamma$ coincidences were used to generate a time-walk curve with 344.3 keV as the reference energy by correcting the centroids of the time-difference spectra by the known lifetime of 46.2(39) ps [26]. A calibration point at the reference energy of 344.3 keV itself with zero relative time walk is also acquired. Next, this process was repeated to generate a time-walk curve with 244.7 keV as the reference energy using feeders to the 366.5-keV state in ^{152}Sm (83.2(9) ps lifetime) [26]. A constant shift, which corresponds to the difference in time walk at 244.7 keV and 344.3 keV, was then applied to the points on the 244.7-keV curve to align them

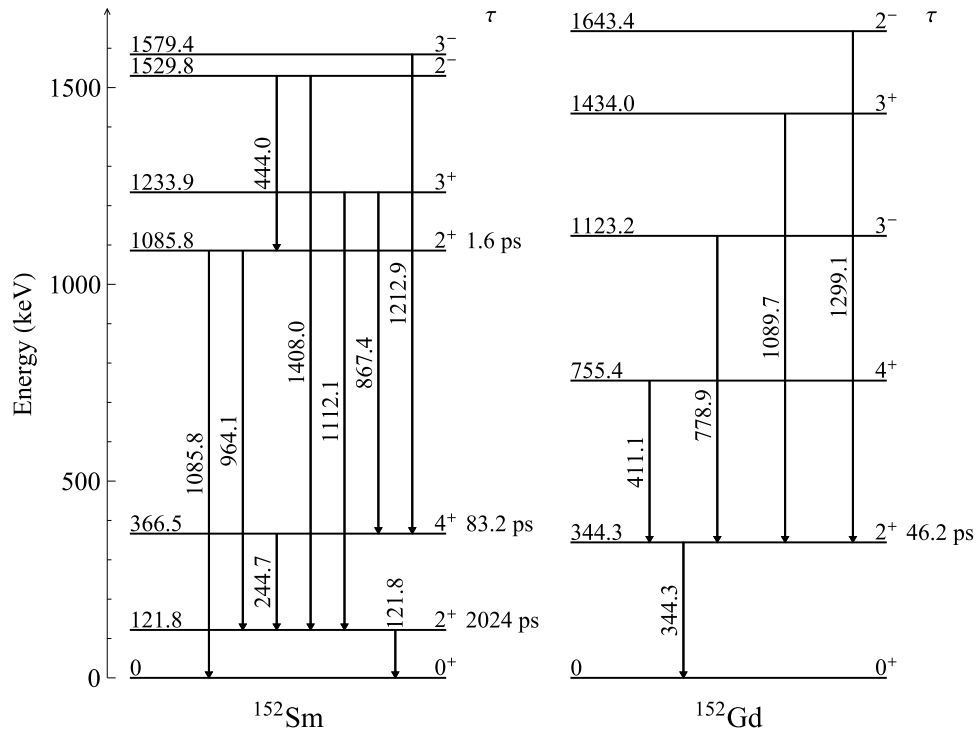


Fig. 4. Partial level schemes for ^{152}Sm and ^{152}Gd following β^- and electron-capture decays, respectively, of a standard ^{152}Eu source. Lifetimes and energies for levels and transitions are taken from Ref. [26].

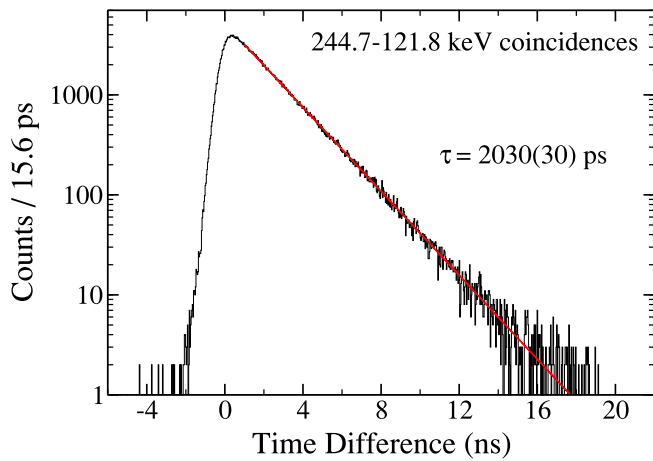


Fig. 5. Lifetime of the 121.8-keV state in ^{152}Sm from fitting an exponential curve (shown in red) to the time-difference spectrum for 244.7–121.8 keV coincidences. The reported uncertainty was derived by fitting different binnings of the time-difference data over a variety of fit ranges. (For interpretation of the references to color in this figure legend, the reader is referred to the web version of this article.)

with the 344.3-keV curve. Additional points using coincidences with the 121.8-keV and 444.0-keV transitions in ^{152}Sm were also utilized. The resultant time-walk curve is shown in Fig. 6 and is parameterized as suggested in Ref. [29] through

$$TW(E) = \frac{a}{\sqrt{E+b}} + cE + d, \quad (2)$$

where a, b, c, and d are fit parameters. The values of the parameters and the shifts used to align the data points with different reference energies were varied in the fit.

In order to perform an independent measurement of the lifetime of the 344.3-keV level in ^{152}Gd , the points in the time-walk curve of Fig. 6 found from coincidences with the 344.3-keV transition were removed

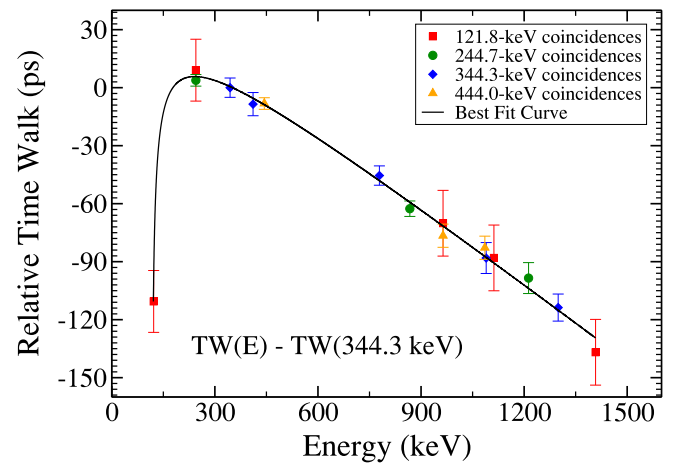


Fig. 6. Time-walk calibration curve with 344.3 keV as the reference energy. Time-walk data with 121.8, 244.7, and 444.0 keV as the reference energies have been shifted to align with the 344.3-keV curve. The best-fit curve to all data points has a root-mean-square deviation of 3 ps. For coincidences with reference energies, the error bars are the centroid fit uncertainties added in quadrature with the uncertainties of the known lifetimes. For the reference energies themselves, the 3 ps RMS deviation added in quadrature with the lifetime uncertainties was used for the error bars.

and the remaining data were fit with a new time-walk curve. Using Eq. (1), the lifetime was found using the centroid of the timing difference spectrum and the time-walk values from the new calibration curve at the feeder and decay energies. The uncertainty in lifetime was calculated using the uncertainty in the centroid fit added in quadrature with the uncertainties in time walk at the feeder and decay energies, which were both taken as 4 ps, the RMS deviation for the new best-fit curve. This process of removing points from the calibration to enable independent lifetime measurements was then repeated for the 366.5-keV and 1085.8-keV states in ^{152}Sm . The RMS deviation of the new time-walk curves was 3 ps for both cases. Fig. 7 shows example time-difference spectra.

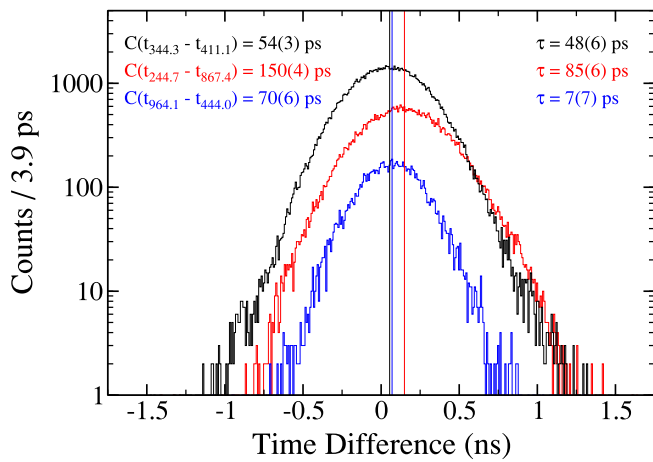


Fig. 7. Centroids of the time-difference spectra for 411.1–344.3 keV (black), 877.4–244.7 keV (red), and 444.0–964.1 keV (blue) coincidences. Lifetimes are calculated by correcting the centroid for the time-walk values at the feeder and decay energies. (For interpretation of the references to color in this figure legend, the reader is referred to the web version of this article.)

Table 1

Lifetimes for excited states in ^{152}Sm and ^{152}Gd . The lifetime of the 121.8-keV level of ^{152}Sm was found using the slope method while the lifetimes of the other levels were extracted from the centroids of time-difference spectra corrected for time walk using the method presented in Ref. [28]. Literature values for the lifetimes are taken from Ref. [26].

Nucleus, Level (keV)	Cascade (keV-keV)	τ_{exp} (ps)	τ_{lit} (ps)
^{152}Sm , 121.8	244.7–121.8	2030(30)	
	964.1–121.8	2020(40)	
	1112.1–121.8	2050(40)	
	1408.0–121.8	2030(40)	
	Average	2030(20)	2024(16)
^{152}Gd , 344.3	411.1–344.3	48(6)	
	778.9–344.3	43(5)	
	1089.7–344.3	46(8)	
	1299.1–344.3	44(7)	
	Average	45(3)	46.2(39)
^{152}Sm , 366.5	867.4–244.7	85(6)	
	1212.9–244.7	76(9)	
	Average	82(5)	83.2(9)
^{152}Sm , 1085.8	444.0–964.1	7(7)	
	444.0–1085.8	–3(7)	
	Average	2(5)	1.6(2)

As seen in Table 1, there is excellent agreement between the extracted lifetimes and the known lifetimes for all measurements.

4. Angular correlation measurements

In general, when nuclei de-excite by undergoing multiple γ -ray decays in cascade, there is an anisotropy in the angular correlations of the emitted photons. The angular correlation of two successive γ rays can be expressed as

$$W(\theta) = 1 + \sum_{i=1}^{\lambda} a_{2i} \cos^{2i} \theta, \quad (3)$$

where the coefficients a_{2i} depend on the spins and parities of the states in the cascade and λ is the lowest multipolarity of the transitions involved [30–32].

In order to test the sensitivity of the array to the angular correlations of successively emitted γ rays, the 1173.2–1332.5 keV cascade in ^{60}Ni populated from ^{60}Co β^- decay was investigated both experimentally and through simulation using GEANT4. First, the number of counts at each of the eight unique angle differences provided by detector pairs in the array of $\text{LaBr}_3(\text{Ce})$ detectors was determined by tallying 1173.2–1332.5 keV

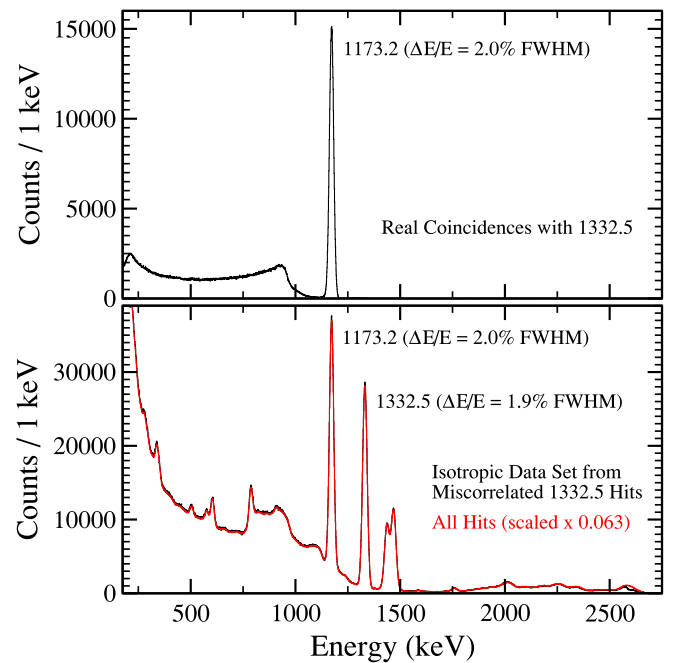


Fig. 8. Top: real coincidences with 1332.5-keV hits. The 1173.2–1332.5 keV coincidence is clearly visible. Bottom: the isotropic data set (black) constructed by intentionally miscalculating 1332.5-keV hits in the current event with the hits in the event prior to the previous event. The energy spectrum of the isotropic set compares well with the energy spectrum of all hits (red), as expected. Unlabeled features originate from room background and the self-activity of the $\text{LaBr}_3(\text{Ce})$ detectors arising from the decays of ^{138}La and ^{227}Ac [21]. (For interpretation of the references to color in this figure legend, the reader is referred to the web version of this article.)

coincidences. The values for the angle differences were taken from the GEANT4 simulation described in the next paragraph.

To correct for disparities in detector efficiencies, the array's response to isotropic data was evaluated by constructing a set of angle differences from uncorrelated 1173.2–1332.5 keV hits. This was done by intentionally miscalculating 1332.5-keV hits in the current event with all hits from the event before the previous event. Since the event window was set to 256 ns, a 1332.5-keV hit at the beginning of the current event is separated in time by at least 256 ns plus the conversion time of the data acquisition system from a hit at the end of the event for correlation. Therefore, the angles between the 1332.5-keV hit in the current event and any 1173.2-keV hits in the older event are random. See Fig. 8 for a comparison of the real and intentionally miscalculated coincidences with 1332.5-keV hits. The number of counts at each angle for real coincidences was then divided by the isotropic data, scaled to correct for count difference. The resulting spectrum was normalized and fit to the form of Eq. (3) (see Fig. 9).

Next, a GEANT4 model of the $\text{LaBr}_3(\text{Ce})$ crystals was implemented. Assuming the first transition is of pure electric quadrupole ($E2$) character, the angular correlation for the 1173.2–1332.5 keV cascade in ^{60}Ni ($4^+ \rightarrow 2^+ \rightarrow 0^+$) is $W(\theta) = 1 + \frac{1}{8} \cos^2 \theta + \frac{1}{24} \cos^4 \theta$. Two billion events that produce this theoretical angular correlation were simulated using GEANT4 and the number of 1173.2–1332.5 keV coincidences at each angle difference was recorded. For both the experimental and simulated data, the angles plotted in Fig. 9 were taken as the average angles leading to 1173.2–1332.5 keV coincidences in the simulation (see Fig. 10). These average angles agree with the geometric angles calculated assuming the γ -ray interactions occur in the center of the crystals to within 2%. The simulation was then repeated using a set of events producing an isotropic angular correlation. The number of coincidences at each angle difference found with the real angular correlation was divided by the corresponding coincidences from the isotropic data, corrected for the normalization of $W(\theta)$, to allow for a

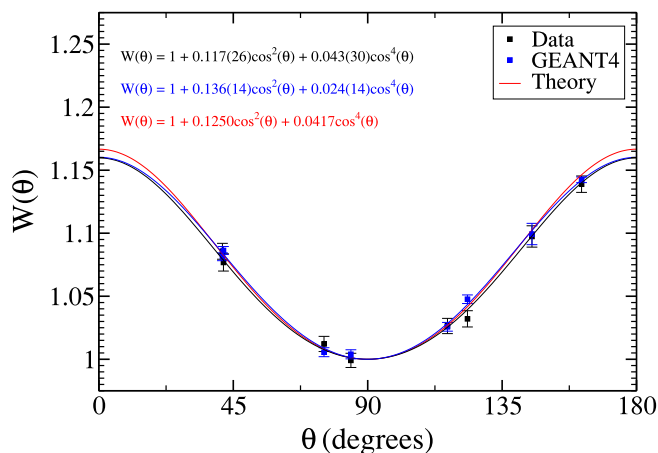


Fig. 9. Experimental angular correlation (black) compared to the angular correlation from GEANT4 simulation (blue) and the theoretical angular correlation (red) for the 1173.2–1332.5 keV cascade in ^{60}Ni . The angular correlation for experiment and simulation is slightly attenuated compared to the theoretical angular correlation because of the finite size of the detectors. The error bars are statistical. (For interpretation of the references to color in this figure legend, the reader is referred to the web version of this article.)

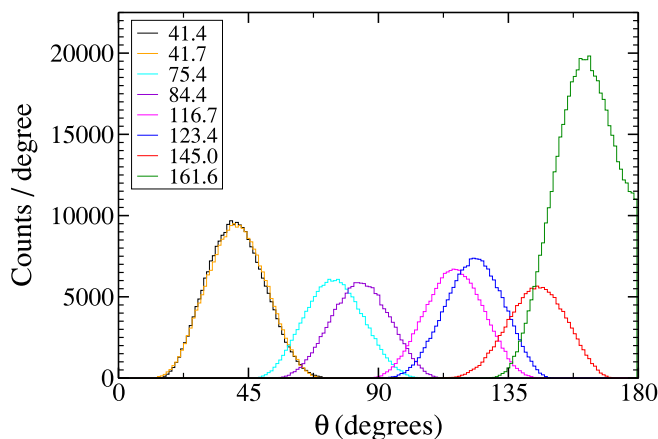


Fig. 10. Angle differences leading to 1173.2–1332.5 keV coincidences in the GEANT4 simulation of two billion $\gamma\gamma$ events. The averages for each unique detector combination were used as the angles in determining both the experimental and simulated angular correlations. The spectrum with an average of 161.6 degrees is not symmetric because the angle between the momentum vectors of the γ rays cannot be larger than 180 degrees. (For interpretation of the references to color in this figure legend, the reader is referred to the web version of this article.)

comparison to the experimental data. As seen in Fig. 9, the experimental and simulated data are in good agreement. The angular correlations derived from experiment and GEANT4 are slightly attenuated with respect to the theoretical angular correlation due to the solid-angle coverage of the detectors.

The same analysis was then repeated for the 898.0–1836.1 keV cascade in ^{88}Sr . The 2734.1-keV state in ^{88}Sr is populated with a 94.4% branching ratio from the electron-capture decay of ^{88}Y [33]. The theoretical angular correlation for this $3^- \rightarrow 2^+ \rightarrow 0^+$ cascade is $W(\theta) = 1 - \frac{3}{20} \cos^2 \theta$, assuming pure electric dipole ($E1$) character for the first transition. Results for the angular correlation derived from the experimental data and the GEANT4 simulation are provided in Fig. 11. As with results for the 1173.2–1332.5 keV, the experimental and simulated angular correlations are in good agreement and are attenuated compared to the theoretical angular correlation since the $\text{LaBr}_3(\text{Ce})$

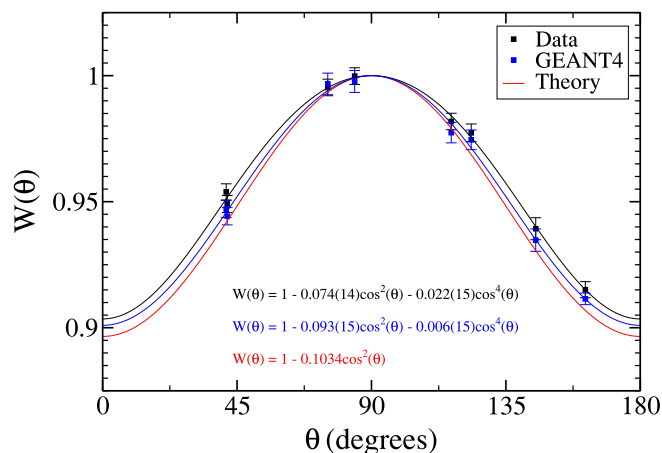


Fig. 11. Experimental angular correlation (black) compared to the angular correlation from GEANT4 simulation (blue) and the theoretical angular correlation (red) for the 898.0–1836.1 keV cascade in ^{88}Sr . The angular correlation for experiment and simulation is slightly attenuated compared to the theoretical angular correlation because of the finite size of the detectors. The error bars are statistical. (For interpretation of the references to color in this figure legend, the reader is referred to the web version of this article.)

crystals are not point detectors at the center angle. In addition, the ^{88}Y source was used to measure the efficiency of the array for this experimental setup. The efficiency was found to be approximately 5.9% at 898.0 keV and 2.8% at 1836.1 keV.

5. Summary

The full array of 16 Saint-Gobain BrillanCe 380 $\text{LaBr}_3(\text{Ce})$ scintillators available at the National Superconducting Cyclotron Laboratory was commissioned together with its electronics setup in a series of lifetime and angular correlation measurements using ^{60}Co , ^{88}Y , and ^{152}Eu sources. Using the ^{60}Co source, the energy resolution of the array at 1173.2 and 1332.5 keV was measured at 2.0% and 1.9% FWHM, respectively, and the FWHM timing resolution was found to be 310 ps for 1173.2–1332.5 keV coincidences. The efficiency of the array was measured to be approximately 5.9% at 898.0 keV and 2.8% at 1836.1 keV. Next, the lifetime of the 121.8-keV level in ^{152}Sm was measured via the exponential slope method using coincidences with several feeder states to be 2030(20) ps, in good agreement with the literature value. In addition, the lifetimes of the 344.3-keV state in ^{152}Gd and the 366.5-keV and 1085.8-keV states in ^{152}Sm were measured using the centroids of time-difference spectra taken from the energy–energy–time difference cube constructed according to Ref. [28]. The agreement of the extracted lifetimes of 45(3), 82(5), and 2(5) ps with their respective literature values demonstrates the applicability of the array for $\gamma\gamma$ fast-timing measurements on the scale of several 10 ps. Finally, the sensitivity of the array to the angular correlations of successively emitted γ rays was investigated using the 1173.2–1332.5 keV cascade in ^{60}Ni and the 898.0–1836.1 keV cascade in ^{88}Sr . The experimentally measured angular correlations were consistent with GEANT4 simulations of the array’s response to γ -ray pairs emitted with the theoretical angular correlations. The successful commissioning measurements indicate that the $\text{LaBr}_3(\text{Ce})$ detectors and electronics are ready to be used in conjunction with other detector systems in experiments.

Acknowledgments

This work was supported by the DOE National Nuclear Security Administration, USA through the Nuclear Science and Security Consortium under Award No. DE-NA0003180. This work was supported in part by the National Science Foundation, USA under Contract No.

PHY-1565546. The authors thank E. Lunderberg for assistance in the beginning stages of the project.

References

- [1] P.H. Regan, R. Shearman, T. Daniel, G. Lorusso, S.M. Collins, S.M. Judge, S.J. Bell, A.K. Pearce, L.A. Gurgi, M. Rudigier, Zs. Podolyák, N. Mărginean, R. Mărginean, S. Kisyov, *J. Phys.: Conf. Ser.* 763 (2016) 012004.
- [2] E.V.D. van Loef, P. Dorenbos, C.W.E. van Eijk, K. Krämer, H.U. Güdel, *Appl. Phys. Lett.* 79 (2001) 1573.
- [3] E.V.D. van Loef, P. Dorenbos, C.W.E. van Eijk, K.W. Krämer, H.U. Güdel, *Nucl. Instrum. Methods Phys. Res. A* 486 (2002) 254.
- [4] K.S. Shah, J. Glodo, M. Klugerman, W.W. Moses, S.E. Derenzo, M.J. Weber, *IEEE Trans. Nucl. Sci.* NS 50 (2003) 2410.
- [5] N. Mărginean, D.L. Balabanski, D. Bucurescu, S. Lalkovski, L. Atanasova, G. Căta-Danil, I. Căta-Danil, J.M. Daugas, D. Deleanu, P. Detistov, G. Deyanova, D. Filipescu, G. Georgiev, D. Ghiță, K.A. Gladnishi, R. Lozeva, T. Glodariu, M. Ivașcu, S. Kisyov, C. Mihai, R. Mărginean, A. Negret, S. Pascu, D. Radulov, T. Sava, L. Stroe, G. Suliman, N.V. Zamfir, *Eur. Phys. J. A* 46 (2010) 329.
- [6] D. Bucurescu, I. Căta-Danil, G. Ciocan, C. Costache, D. Deleanu, R. Dima, D. Filipescu, N. Florea, D.G. Ghiță, T. Glodariu, M. Ivașcu, R. Lică, N. Mărginean, R. Mărginean, C. Mihai, A. Negret, C.R. Niță, A. Olăcel, S. Pascu, T. Sava, L. Stroe, A. Șerban, R. Șuvăilă, S. Toma, N.V. Zamfir, G. Căta-Danil, I. Gheorghie, I.O. Mitu, G. Suliman, C.A. Ur, T. Braunroth, A. Dewald, C. Fransen, A.M. Bruce, Zs. Podolyák, P.H. Regan, O.J. Roberts, *Nucl. Instrum. Methods Phys. Res. A* 837 (2016) 1.
- [7] O.J. Roberts, A.M. Bruce, P.H. Regan, Zs. Podolyák, C.M. Townsley, J.F. Smith, K.F. Mulholland, A. Smith, *Nucl. Instrum. Methods Phys. Res. A* 748 (2014) 91.
- [8] J.-M. Régis, G.S. Simpson, A. Blanc, G. de France, M. Jentschel, U. Köster, P. Mutti, V. Pazyi, N. Saed-Samii, T. Soldner, C.A. Ur, W. Urban, A.M. Bruce, F. Drouet, L.M. Fraile, S. Ilieva, J. Jolie, W. Korten, T. Kröll, S. Lalkovski, H. Mach, N. Mărginean, G. Pascovici, Zs. Podolyák, P.H. Regan, O.J. Roberts, J.F. Smith, C. Townsley, A. Vancraeynest, N. Warr, *Nucl. Instrum. Methods Phys. Res. A* 763 (2014) 210.
- [9] Z. Patel, F. Browne, A.M. Bruce, N. Chiga, R. Daido, S. Nishimura, Zs. Podolyák, P.H. Regan, O.J. Roberts, H. Sakurai, P.-A. Söderström, T. Sumikama, H. Watanabe, *RIKEN Accel. Prog. Rep.* 47 (2014) 13.
- [10] F. Browne, A.M. Bruce, T. Sumikama, I. Nishizuka, S. Nishimura, P. Doornenbal, G. Lorusso, P.-A. Söderström, H. Watanabe, R. Daido, Z. Patel, S. Rice, L. Sinclair, J. Wu, Z.Y. Xu, A. Yagi, H. Baba, N. Chiga, R. Carroll, F. Didierjean, Y. Fang, N. Fukuda, G. Gey, E. Ideguchi, N. Inabe, T. Isobe, D. Kameda, I. Kojouharov, N. Kurz, T. Kubo, S. Lalkovski, Z. Li, R. Lozeva, H. Nishibata, A. Odahara, Zs. Podolyák, P.H. Regan, O.J. Roberts, H. Sakurai, H. Schaffner, G.S. Simpson, H. Suzuki, H. Takeda, M. Tanaka, J. Taprogge, V. Werner, O. Wieland, *Phys. Lett. B* 750 (2015) 448.
- [11] M. Heine, S. Courtin, G. Fruet, D.G. Jenkins, L. Morris, D. Montanari, M. Rudigier, P. Adsley, D. Curien, S. Della Negra, J. Lesrel, C. Beck, L. Charles, P. Dené, F. Haas, F. Hammache, G. Heitz, M. Krauth, A. Meyer, Zs. Podolyák, P.H. Regan, M. Richer, N. de Séréville, C. Stodel, *Nucl. Instrum. Methods Phys. Res. A* 903 (2018) 1.
- [12] S. Zhu, F.G. Kondev, M.P. Carpenter, I. Ahmad, C.J. Chiara, J.P. Greene, G. Gurdal, R.V.F. Janssens, S. Lalkovski, T. Lauritsen, D. Seweryniak, *Nucl. Instrum. Methods Phys. Res. A* 652 (2011) 231.
- [13] M. Rudigier, S. Lalkovski, E.R. Gamba, A.M. Bruce, Zs. Podolyák, P.H. Regan, M. Carpenter, S. Zhu, A.D. Ayangeakaa, J.T. Anderson, T. Berry, S. Bottoni, I. Burrows, R. Carroll, P. Copp, D. Cullen, T. Daniel, L. Fraile, M. Carmona Gallardo, A. Grant, J.P. Greene, L.A. Guegi, D. Hartley, R. Ilieva, S. Ilieva, R.V.F. Janssens, F.G. Kondev, T. Kröll, G.J. Lane, T. Lauritsen, I. Lazarus, G. Lotay, G. Fernandez Martinez, V. Pucknell, M. Reed, J. Rohrer, J. Sethi, D. Seweryniak, C.M. Shand, J. Simpson, M. Smolen, E. Stefanova, V. Vedia, O. Yordanov, *Acta Phys. Polon. B* 48 (2017) 351.
- [14] E.R. Gamba, A.M. Bruce, M. Rudigier, S. Lalkovski, S. Bottoni, M.P. Carpenter, S. Zhu, A.D. Ayangeakaa, J.T. Anderson, T.A. Berry, I. Burrows, R.J. Carrol, P. Copp, M. Carmona Gallardo, D.M. Cullen, T. Daniel, G. Fernández Martínez, J.P. Greene, L.A. Gurgi, D.J. Hartley, R. Ilieva, S. Ilieva, R.V.F. Janssens, F.G. Kondev, T. Kröll, G.J. Lane, T. Lauritsen, I. Lazarus, G. Lotay, C.R. Ni, Zs. Podolyák, V. Pucknell, M. Reed, P.H. Regan, J. Rohrer, J. Sethi, D. Seweryniak, C.M. Shand, J. Simpson, M. Smolén, V. Vedia, E.A. Stefanova, O. Yordanov, *Acta Phys. Polon. B* 49 (2018) 555.
- [15] R. Shearman, S.M. Collins, G. Lorusso, M. Rudigier, S.M. Judge, S.J. Bell, Zs. Podolyák, P.H. Regan, *Radiat. Phys. Chem.* 140 (2017) 475.
- [16] S.M. Collins, R. Shearman, J.D. Keightley, P.H. Regan, *Appl. Radiat. Isot.* 134 (2018) 290.
- [17] A. Gade, B.M. Sherrill, *Phys. Scr.* 91 (2016) 053003.
- [18] D. Weisshaar, M.S. Wallace, P. Adrich, D. Bazin, C.M. Campbell, J.M. Cook, S. Ettenauer, A. Gade, T. Glasmacher, S. McDaniel, A. Obertelli, A. Ratkiewicz, A.M. Rogers, K. Siwek, S.R. Tornga, *Nucl. Instrum. Methods Phys. Res. A* 594 (2008) 56.
- [19] C.J. Prokop, S.N. Liddick, N.R. Larson, S. Suchyta, J.R. Tompkins, *Nucl. Instrum. Methods Phys. Res. A* 792 (2015) 81.
- [20] B.P. Crider, C.J. Prokop, S.N. Liddick, M. Al-Shudifat, A.D. Ayangeakaa, M.P. Carpenter, J.J. Carroll, J. Chen, C.J. Chiara, H.M. David, A.C. Dombos, S. Go, R. Grzywacz, J. Harker, R.V.F. Janssens, N. Larson, T. Lauritsen, R. Lewis, S.J. Quinn, F. Recchia, A. Spyrou, S. Suchyta, W.B. Walters, S. Zhu, *Phys. Lett. B* 763 (2016) 108.
- [21] Saint-Gobain Crystals, **BrillanCe Scintillators Performance Summary, 2009.** <https://www.crystals.saint-gobain.com/sites/imdf.crystals.com/files/documents/brilliance-scintillators-performance-summary.pdf>.
- [22] W.F. Mueller, J.A. Church, T. Glasmacher, D. Gutknecht, G. Hackman, P.G. Hansen, Z. Hu, K.L. Miller, P. Quirin, *Nucl. Instrum. Methods Phys. Res. A* 466 (2001) 492.
- [23] Mesytec, 2018. <http://www.mesytec.com/product-list.html>.
- [24] P.C. Bender, GRUTinizer, GitHub repository, 2018. <https://www.github.com/pcbend/GRUTinizer/>.
- [25] E. Browne, J.K. Tuli, *Nucl. Data Sheets* 114 (2013) 1849.
- [26] M.J. Martin, *Nucl. Data Sheets* 114 (2013) 1497.
- [27] J.-M. Régis, H. Mach, G.S. Simpson, J. Jolie, G. Pascovici, N. Saed-Samii, N. Warr, A. Bruce, J. Degenkolb, L.M. Fraile, C. Fransen, D.G. Ghita, S. Kisyov, U. Koester, A. Korgul, S. Lalkovski, N. Mărginean, P. Mutti, B. Olaizola, Z. Podolyák, P.H. Regan, O.J. Roberts, M. Rudigier, L. Stroe, W. Urban, D. Wilmsen, *Nucl. Instrum. Methods Phys. Res. A* 726 (2013) 191.
- [28] J.-M. Régis, M. Dannhoff, J. Jolie, *Nucl. Instrum. Methods Phys. Res. A* (2018) 38.
- [29] J.-M. Régis, M. Rudigier, J. Jolie, A. Blazhev, C. Fransen, G. Pascovici, N. Warr, *Nucl. Instrum. Methods Phys. Res. A* 684 (2012) 36.
- [30] D.R. Hamilton, *Phys. Rev.* 58 (1940) 122.
- [31] G. Goertzel, *Phys. Rev.* 70 (1946) 897.
- [32] E.L. Brady, M. Deutsch, *Phys. Rev.* 78 (1950) 558.
- [33] E.A. McCutchan, A.A. Sonzogni, *Nucl. Data Sheets* 115 (2014) 134.